Estimation of fracture flow parameters through numerical analysis of hydromechanical pressure pulses

F. Cappa, Y. Guglielmi, J. Rutqvist, C.-F. Tsang, A. Thoraval

Estimation of fracture flow parameters through numerical analysis of hydromechanical pressure pulses

Frédéric Cappa [1,*], Yves Guglielmi [2], Jonny Rutqvist [3], Chin-Fu Tsang [3], and Alain Thoraval [4]

[1] Géosciences Azur, University of Nice Sophia-Antipolis, Sophia-Antipolis, France

[2] Géologie des Systèmes et des Réservoirs Carbonatés, University of Provence Aix-Marseille, France

[3] Earth Sciences Division, Lawrence Berkeley National Laboratory, Berkeley, USA

[4] INERIS, Ecole National Supérieure des Mines de Nancy, Parc de Saurupt, Nancy, France

* Corresponding author. Fax: (+ 33) 4.92.94.26.10

E-mail address: cappa@geoazur.unice.fr (F. Cappa)

Abstract

The flow parameters of a natural fracture were estimated by modelling *in situ* pressure pulses. The pulses were generated in two horizontal boreholes spaced 1 m apart vertically and intersecting a near-vertical highly permeable fracture located within a shallow fractured carbonate reservoir. Fracture hydromechanical response was monitored using specialized fiber-optic borehole equipment that could simultaneously measure fluid pressure and fracture displacements. Measurements indicated a significant time lag between the pressure peak at the injection point and the one at the second measuring point, located 1 m away. The pressure pulse dilated and contracted the fracture. Field data were analyzed through hydraulic and coupled hydromechanical simulations using different governing flow laws. In matching the time lag between the pressure peaks at the two measuring points, our hydraulic models indicated that (1) flow was channeled in the fracture, (2) the hydraulic conductivity tensor was highly anisotropic, and (3) the radius of pulse influence was asymmetric, in that the pulse travelled faster vertically than horizontally. Moreover, our parametric study demonstrated that the fluid pressure diffusion through the fracture was quite sensitive to the spacing and orientation of channels, hydraulic aperture, storativity and hydraulic conductivity. Comparison between hydraulic and hydromechanical models showed that the deformation significantly affected fracture permeability and storativity, and consequently, the fluid pressure propagation, suggesting that the simultaneous measurements of pressure and mechanical displacement signals could substantially improve the interpretation of pulse tests during reservoir characterization.

Key words: Fractures, Pressure pulse, Deformation, Hydromechanical coupling, Numerical simulations

1. Introduction

Understanding hydromechanical effects within fractured media has become a major field of scientific interest in geosciences [*Tsang*, 1999]. Notably, the impact of dynamic changes caused by fluid pressure or stress on fracture behavior has prime importance for hydrogeology, seismology, and geomechanics.

In fractured rock, fluid flow and storage occur mainly in the fractures, which are embedded into rock matrix blocks of very low permeability [*Bruel et al.*, 1994]. Fluid flow in such fractured rock is often complex due to heterogeneities, both at the scale of the single fracture and the entire fracture network. Numerous laboratory, field, and modelling investigations have shown that fluid flow in a single deformable fracture can depend on a number of factors such as the fracture hydraulic and mechanical parameters, the effective stresses applied on the fracture plane, the amount of surface contact area and voids, and channelling [*Rutqvist and Stephansson*, 2003]. For example, any variation in stress on fracture changes the geometry of its void space, which in turn changes its global permeability and preferential flow paths [*Pyrak-Nolte and Morris*, 2000]. Thus, the fluid dynamics of fractured rock depend both on mechanical and hydraulic processes, which are intimately linked through hydromechanical coupling phenomena.

At the scale of a fracture network, the complex geometry and the great variability in properties, such as fracture aperture and stiffness, complicate the understanding of interactions between groundwater flow and mechanical processes [*Cappa et al.*, 2005]. When fractures are highly permeable, the hydromechanical effects are then half-coupled, with hydraulic processes exclusively interacting mechanical processes. When the fractures are tight, the coupling is generally complete and occurs through fracture-fluid and deformation interactions.

To improve understanding of the relationship between hydraulic and mechanical processes in fractured rock, several recent studies have used coupled hydromechanical modelling of hydraulic-field tests combined with fracture-mechanical displacement measurements [*Rutqvist et al.*, 1998; *Cappa et al.*, 2005; *Cappa et al.*, 2006b; *Murdoch and Germanovich*, 2006; *Svenson et al.*, 2007]. Still, despite these recent tests, field tests on single fractures, or within a fracture network that measure simultaneously both hydraulic and mechanical responses are comparatively rare [*Gale*, 1975; *Martin et al.*, 1990; *Gertsch*, 1990; *Myer*, 1991; *Schweisinger and Murdoch*, 2002; *Cappa et al.*, 2005; *Murdoch and Germanovich*, 2006; *Cappa et al.*, 2006a; *Cappa et al.*, 2006b; *Svenson et al.*, 2007]. Moreover, *in situ* behavior of fractures is often taken to be mainly dependent on scale effects and the overall complexity of the fracture network. As a result, the geometries of single fractures are currently simplified using a parallel plate model. Consequently, imaging and monitoring these coupled processes in-situ, and developing the coupling relations between them remain major challenges. It is commonly recognized that there is a lack of in-situ data that could help us understand the processes at the mesoscale (which is the tenth-of-meters scale of large fracture zones). The main reason for this lack is that such data are difficult to obtain at depths exceeding 300 m, due to technological difficulties and cost.

In this paper, we present the results from hydraulic and coupled hydromechanical simulations using different governing flow laws to analyze a unique data set of fluid pressure and fracture displacement signals taken during a pulse test. These measurements allowed us to accurately explore fluid flow in a fracture plane. The present study extends previous simulation studies of hydromechanical processes in the fracture network within a carbonate reservoir [*Cappa et al.*, 2005; *Cappa et al.*, 2006b] to an analysis of flow parameters controlling hydraulic communications in a highly permeable, highly deformable fracture plane. In these previous studies, Cappa et al. [*2006b*] found that pulse testing with high-

frequency measurements of fluid pressure and mechanical displacement is a useful new method for *in situ* determining hydraulic aperture and the normal stiffness of fractures, as well as the equivalent stiffness of the surrounding rock mass. They also found that, with this method, potential misinterpretations of fracture hydraulic aperture by conventional curve matching of pulse-pressure data can be avoided with an appropriate numerical analysis of the complete pressure-time and displacement-time curves, including results from both the pressure-increasing and pressure-decreasing stages. Compared to standard analytical pulse-test approaches, this new method showed that ignoring coupled hydromechanical effects could lead to a 25% error in estimating fracture hydraulic properties [*Cappa et al.*, 2006b]. Order-of-magnitude contrasts of 10 to 1000 in both hydraulic and mechanical properties were determined among the reservoir fractures, and it was shown that these contrasts controlled the mesoscale hydromechanical behavior of the reservoir. Those results were based on a variety of hydromechanical simulations considering the modified cubic law [*Witherspoon et al.*, 1980] as the governing flow equation to evaluate the curves of fracture normal displacement as a function of fluid pressure, measured at the same borehole during pulse tests. Hydraulic communications complexity within the fracture plane were not investigated. In the study presented herein, we introduce new results from numerical simulations related to how hydraulic and geometrical parameters in the pressurized fracture plane influence fluid flow. Compared to the previous study of Cappa et al. [*2006b*], here we analyse the pressure variations and time lag between pressure peaks measured at two points in the fracture using different flow models.

After providing a brief review of flow concepts and governing equations for fractures, we introduce the data set used in this paper. We describe simultaneous *in situ* measurements of fluid pressure and fracture-normal displacements during pressure pulses applied to a single near-vertical fracture within a high-permeability fracture network. The pulses were generated

in two horizontal boreholes spaced 1m apart vertically. Such protocol enables us to investigate the hydromechanical effects within a small fracture area of a few square meters. These field data were then analyzed using two numerical approaches:

- Hydraulic simulations, ignoring the effect of deformation, were carried out to estimate flow parameters using both a parallel plate model and a channeling model of the pressurized fracture. In this hydraulic analysis, fracture hydraulic aperture, storativity and the hydraulic conductivity tensor were calculated.
- Hydromechanical simulations were then performed to analyze the influence of deformation and the amount of contact areas within the fracture on its hydromechanical response.

Finally, based on a comparison of our modelling results, we provide a discussion and concluding remarks for the issues raised by our findings.

2.Fluid Flow and Hydromechanical Coupling in a Rock Fracture: Governing Equations

2.1. Fracture Fluid Flow

In a natural fracture, fluid flow occurs through interconnected voids between two rough rock surfaces in partial contact. Voids can be of variable geometry and aperture. Fluid flow is greatest through those channels that have the largest apertures, and least through the contact areas [*Zimmerman et al.*, 1992]. As a first approximation, the fluid flow along a fracture is modelled as flow between two parallel plates with constant hydraulic aperture (b_h) described by the "cubic law" [*Snow*, 1965; *Louis and Maini*, 1970]:

$$q = \frac{b_h^{\,3} w \rho g}{12\mu} \Delta H \qquad (1)$$

where q is the flow rate per unit width *(w)*, ρ is the fluid density, g is the gravitational acceleration, μ is the fluid dynamic viscosity, and ΔH is the hydraulic head gradient.

Also, analogously to the hydraulic behavior in a porous reservoir, transient fluid flow in a fracture with uniform aperture can be modelled using the diffusivity equation written in terms of hydraulic head *(H)*:

$$\frac{\delta H}{\delta t} = D.\nabla^2 H \tag{2}$$

where ∇^2 is the Laplace operator, t is the time, and D is the fracture hydraulic diffusivity given by:

$$D = \frac{K}{S_i} = \frac{T}{S} \tag{3}$$

where K is hydraulic conductivity, S_i is intrinsic storativity, and T is transmissivity, which can be defined according to the parallel plate flow concept as:

$$T = \frac{b_h{}^3 g\rho}{12\mu} \tag{4}$$

In terms of hydraulic concepts, the storativity *(S)* expresses the increase in the weight of fluid stored per unit area of a fracture in response to a unit increase in pressure and can be defined according to [*Dominenco and Schwartz* 1990]:

$$S_h = \frac{1}{A}\frac{\partial(\rho g V_f)}{\partial P_f} \tag{5}$$

where A is the area of the fracture plane, P_f is the fluid pressure and V_f is the fluid volume between the two fracture faces. This fracture storativity *(S)* is noted as a hydraulic storativity *(S_h)* because this formulation depends exclusively on the fluid properties and the fracture dimension.

2.2. Fracture Elastic Hydromechanical Behavior

Most hydromechanical models have been developed from laboratory experiments and describe fracture hydromechanical behavior as a function of normal stress [*Rutqvist and Stephansson* 2003]. Due to the difficulties in developing laboratory measurement facilities during shear-slip experiments, only a few models have been proposed for understanding fracture hydromechanical behavior under shear stress [*Makurat et al.*, 1990; *Olsson and Barton*, 2001].

The most fundamental formulation for describing the coupling between hydraulic and mechanical processes in a geological media is provided by the effective stress law developed by Terzaghi [*1923*] and later modified by Biot [*1941*]. This effective stress law (6) describes the relationship between effective normal stress *(σ'_n)*, normal stress *(σ_n)* and fluid pressure *(P_f)*:

$$\sigma'_n = \sigma_n - \alpha P_f \tag{6}$$

where α is the Biot effective stress constant.

Under normal stress, the parallel-plate flow concept is commonly used to describe the coupling between fracture flow and normal deformation, according to the "modified cubic law" suggested by Witherspoon et al. [*1980*]:

$$q = \frac{(b_{hi} + f\Delta U_n)^3 w\rho g}{12\mu}\Delta H \tag{7}$$

with

$$b_h = b_{hi} + f\Delta U_n \tag{8}$$

where b_{hi} is the initial hydraulic aperture at the initial effective stress and f is a factor reflecting the influence of roughness on the tortuosity of flow. This law associates the fracture hydraulic aperture (b_h) to the fracture normal displacement (U_n) and was verified and validated against numerous laboratory experiments [*Witherspoon et al.*, 1980; *Detournay*, 1980; *Alvarez et al.*, 1985].

Fracture displacements are induced by a change in the effective stress field acting on the fracture. The relationship between stresses and fracture displacement is described by numerous mechanical constitutive laws (e.g., *Goodman*, 1970; *Goodman*, 1974; *Barton et al.*, 1985). The most basic relation between a change in fracture normal and shear displacement (respectively, noted U_n and U_s) caused by a change in effective normal (σ'_n) and shear (σ'_s) stresses is suggested by the Goodman linear equations [*1970*]:

$$\Delta U_n = \frac{\Delta\sigma'_n}{k_n} \tag{9}$$

$$\Delta U_s = \frac{\Delta \sigma_s}{k_s} \tag{10}$$

where k_n and k_s are respectively the normal and shear stiffness. Later, Goodman [*1974*] formulated the first nonlinear joint model with a hyperbolic form, written as:

$$\Delta U_n = \frac{\sigma'_{ni}}{k_{ni}}\left(1 - \frac{\sigma'_{ni}}{\sigma'_n}\right) \tag{11}$$

where k_{ni} and σ'_{ni} are respectively the initial fracture normal stiffness and the initial effective normal stress at initial reference condition.

Many studies show the role of fracture geometry on fluid flow and, in particular, the evolution of flow paths with changes in stress. Pyrak-Nolte and Morris [*2000*] showed that fluid flow and hydromechanical properties through a single fracture under normal stress are implicitly related through the geometry of the void space and contact area that comprise the fracture. In the study of Pyrak-Nolte and Morris [*2000*], fluid flow and fracture displacement are expressed as a function of normal stress through a fracture with variable contact areas and aperture distribution. Based on laboratory hydromechanical experiments under normal stress, Duveau et al. [*1997*] suggested a modified effective stress law, also considering the amount of contact area and the effective normal stress:

$$\sigma'_n = \sigma_n - (1 - S_c)P_f \tag{12}$$

where S_c is the ratio of the contact area to total fracture surface, for a fracture described as a succession of co-planar voids separated by contact areas.

A complete coupled hydromechanical model can be derived from a fracture flow law and a mechanical constitutive law linking the normal displacement and the normal effective stress to obtain a direct relationship between the fracture transmissivity and the normal effective stress. For example, one of the most recent coupled models was proposed by Rutqvist [*1995a*] who combines Goodman's nonlinear mechanical joint model (11) with equations (4) and (8) to derive the following hydromechanical model:

$$T = \frac{\rho g w}{12\mu}\left[b_{hi} + \frac{\sigma'_{ni}}{k_{ni} f^{1/3}}\left(1 - \frac{\sigma'_{ni}}{\sigma'_{n}}\right)\right]^3 \tag{13}$$

Equation (13) shows that the initial hydraulic aperture, initial normal stiffness, and initial stress are important factors defining the relationship between stress and transmissivity of a fracture plane [*Rutqvist*, 1995a].

In a similar approach, the fracture storativity is generally described in terms of elastic storativity (S_e), which accounts for the compressibility of the fracture, the rock matrix and the fluid (C_f). Several relationships were formulated for describing S_e from the coupled hydromechanical behavior of single fracture considered as two parallel plates [*Doe et al.*, 1982; *Rutqvist*, 1995b; *Rutqvist et al.*, 1998; *Bruel*, 2002].

2.3. Flow Pattern within a Fracture and Consequences on Hydromechanical Effects

Many studies of fracture fluid flow are based on the common assumption that a fracture can be represented as two parallel plates in which the flow obeys the cubic law (Eq. 1) [*Zimmermann and Bodvarsson*, 1996]. Nevertheless, this is not consistent with field and laboratory observations of flow channeling in single fractures [*Moreno et al.*, 1985; *Bourke*, 1987; *Gentier et al.*, 2000]. Based on these observations, flow channeling is mainly explained by a variation of apertures and contact areas within the fracture [*Neretnieks et al.*, 1982; *Tsang*

and Tsang, 1987; *Tsang and Tsang*, 1989; *Tsang et al.*, 1988; *Moreno et al.*, 1988; *Moreno et al.*, 1990; *Tsang and Neretnieks*, 1998]. In such fractures, a variable aperture model is often better adapted to describe flow and transport channeling effects than a parallel plate model [*Neretnieks et al.*, 1982; *Bourke*, 1987; *Pyrak-Nolte*, 1988; *Tsang and Tsan*g, 1989; *Tsang et al.*, 2001]. Nevertheless, although fracture apertures can be described by normal, lognormal, gamma distributions or a self-affine scale invariance, researchers often find it convenient to represent aperture fields in terms of equivalent aperture in the parallel plate model [Zheng et al., 2008].

In terms of fracture hydromechanical behavior, the modified cubic law (Eq. 7) is commonly used to describe flow in deformable fractures modelled as two parallel plates. In that case, the effect of channeling is not taken into account. However, the degree of flow channeling also depends on the fracture mechanical evolution [*Zimmerman and Main*, 2004]. Rare are the fully coupled hydromechanical models accounting for the flow channelling effect, which induces a heterogeneous spatial distribution of pressures [*Pyrak-Nolte et al.*, 1987; *Pyrak-Nolte and Morris*, 2000]. Some models accounting for the effects of contact areas on fracture flow and deformability are proposed from laboratory observations [*Yang et al.*, 1989; *Myer*, 1991; *Pyrak-Nolte and Morris*, 2000; *Dewitler et al.*, 2002]. Sibaï et al. [*1997*] and Gentier et al. [*2000*] showed through laboratory hydromechanical experiments that the spatial distribution of contact areas within the fracture vary under normal stress and induce preferential flow paths through localized channels. Recent hydromechanical simulations of flow in a rough deformable fracture confirmed observations of flow channeling, and showed that the distributions of fracture aperture during shearing change and cause significant fluid flow channelling effects [*Koyama et al.*, 2005].

3. Field Hydromechanical Experiment

3.1. Test Site

The experiment consisted of a pulse test that measures fluid pressure and fracture normal displacement at the Coaraze Laboratory site in France (Fig. 1). The Coaraze research project studied coupled groundwater and mechanical processes in complex shallow fractured rock in which fractures are highly permeable and well connected. This is an intermediate scale test site (30 m × 30 m × 15 m) where experimental conditions are well controlled. The fracture network is made up of highly permeable near-vertical faults intersected by low-permeable bedding planes with a dip angle of 45° (Fig. 1). The rock matrix is practically impermeable. Storage only occurs in the fractures. The field experiment simulated in this paper is described in detail in Cappa et al. [*2006b*], and the hydromechanical behavior of the fractured rock mass is presented in Cappa et al. [*2005*].

3.2. Fractures Walls Morphology Characterization

At the scale of the single fracture, faults and bedding planes present different geometrical characteristics. The surface roughness of faults is generally greater than that of bedding planes, with average values of asperity heights of 1.4 mm and 0.5 mm, respectively (CLA index) [*Tse and Curden*, 1979]. Compared to laboratory observations of flow channelling in rough fractures, a fracture with a CLA index of 1.4 mm contains highly conductive preferential flow channels [*Cappa et al.*, 2005]. This is supported by direct physical evidence of clean linear tectonic ridges between channels in fault planes [*Guglielmi et al.*, 2008]. These ridges are in contact and limit voids where fluid can flow.

3.3. Experimental Setup

Two horizontal boreholes (HM1 and HM2 in Fig. 2), spaced 1 m vertically, were drilled normal to the F_{12} near-vertical fault (Fig. 1). Each borehole stopped 10 cm beyond the fault. The exact location of the fault was identified with a televiewer run into the boreholes. In each borehole, the fault was isolated with an inflatable packer to create a 0.4 m long sealed section. In each sealed section, the measurement device consisted of a fiber-optic fluid pressure and a fiber-optic normal displacement sensor fixed to the borehole walls by two anchors located on both sides of the fault (Fig. 2). This device was specially adapted from the BOF-EX device developed by RocTest-Telemac® [*Cappa et al.*, 2006a]. This borehole equipment is capable (with high frequency [120 Hz] and high accuracy) of simultaneously measuring change in fluid pressure (± 1 kPa) and displacement normal to the fault walls (± 1×10^{-7} m) during a fast pulse testing. Compared to classical borehole equipment, in which the pulse sampling frequency is low, a unique feature in the analysis of this pulse injection experiment is that the entire test cycle of both the initial pressure increase and subsequent pressure fall-off is carefully monitored and used for the evaluation of the *in situ* hydromechanical behavior [*Cappa et al.*, 2006a]. Moreover, high-frequency sampling allows measuring, with a high accuracy, the time response between the two instrumented points.

The experiment consisted of a pressure pulse of 86 kPa applied to HM1. The injected fluid volume was 1.2 l. Before the initiation of the pulse, initial pressure values were 39 kPa at HM1 and 27 kPa at HM2.

3.4. Hydromechanical Field Test Results

For a test duration of 40 seconds, the initiation of pulse (t = 0 in Fig. 3) begins 15 seconds after the start of monitoring. At HM1, the pressure change displays a non linear oscillatory behaviour (Fig. 3). Pressure increases from 39 kPa to 125 kPa in 3.5 seconds, and then decreases to reach its initial value in 8 seconds. The normal displacement follows the pressure

change, although the displacement is less oscillatory and more damped compared to pressure. Around the time of peak pressure, the magnitude of normal displacement in HM1 reaches a maximum of 1.9×10^{-6} m. The peak pressure at HM2 is lower than at HM1 ($\Delta P = 22$ kPa instead of 86 kPa) and is reached 1.5 seconds later. At HM2, the pressure decrease is slower than the one at HM1. Normal displacement change at HM2 follows the local pressure change at HM2, with the magnitude of displacement reaching a maximum of 0.45×10^{-6} m.

4. Numerical Simulations of the Measured Pressure Pulse

4.1. Numerical Analysis Methods

Two numerical approaches were used to analyse the pulse test, accounting both for the hydraulic effects and hydromechanical interactions in the pressurized fracture. Two independent codes were used to improve confidence and quality in model results.

- In the first approach, hydraulic simulations, ignoring the effect of mechanical deformation, were conducted to evaluate the pressure changes during the pulse test. In this analysis, results from a model in which the fracture is represented by two parallel plates are compared to results from a channel-network model. The three-dimensional distinct-element code 3DEC [*Cundall*, 1988; *Itasca*, 2003a] was first applied to simulate the parallel plate fracture model (i.e., fracture with a uniform aperture). In the 3DEC code, fracture is modelled as an interface between impervious rock blocks. The flow of fluid in the fracture is laminar and governed by the cubic law (Eq. 1). In the code, the fluid pressure change is calculated as follows:

$$P_f = P_0 + \left(K_f q \frac{\Delta t}{V} \right) - \left(K_f \frac{\Delta V}{V} \right) \tag{14}$$

where P_0 is the initial pressure, K_f is the fluid bulk modulus, q is the flow rate determined from the cubic law, Δt is the time increment, V is the initial fracture volume, and ΔV is the change of volume due to the deformation. Then, we have used the three-dimensional finite element code 3FLO [*Itasca*, 2003b] to simulate a second fracture model in which fluid flows in a channel network arranged within the fracture plane, accordingly to the direct physical evidence of channelling above-mentioned in section 3.2. Between channels, rock matrix is impervious. Channels correspond to fully-saturated mono-dimensional elements (pipes) in which flow is governed by the diffusivity equation (Eq. 2). In this series of hydraulic simulations, fracture hydraulic properties were estimated by matching the measured pressure-versus-time response, and notably, the time lag between the pressure peaks at the two measuring points. Sensitivity of the hydraulic response to various fracture hydraulic parameters, the channel spacing and orientation as well as the geometry of the fracture network was analysed.

- In the second approach, hydromechanical modelling, including the effect of deformation, was conducted with the 3DEC code to analyse the fully coupled flow-deformation processes in the fracture, accounting for the effects of fracture contact areas and the fracture-matrix hydromechanical interactions. The effects of fracture contact areas were considered through the modified effective stress law (Eq. 12) proposed by Duveau et al. [*1997*], and Murdoch and Germanovich [*2006*]. This law was implemented within the 3DEC code, and, verified and validated against laboratory hydromechanical experiments on single deformable fractures [*Sibaï et al.*, 1997]. In the hydromechanical analyses conducted herein, discontinuities and the rock matrix are considered elastic. Fracture deformations and hydraulic apertures are calculated as a function of the effective stresses, assuming a constant normal stiffness for fractures, which can be reasonably admitted due to the infinitesimal strains measured in the experiment.

4.2. Geometry and Initial Conditions

In the numerical analyses conducted herein, the following model geometry and initial conditions were used; in each model, the pressurized fracture has a dip angle of 70° (Fig. 4-5 and Table 1):

- Models (a) and (b) (Fig. 4a and 4b) correspond to a three-dimensional model of the fracture (6 m × 6 m). Model (a) is a parallel plate model of a fracture with a uniform aperture. Model (b) represents the fracture as an interconnected network of orthogonal channels spaced 0.1 m apart. The model size is chosen so the fracture is in the saturated zone of the site.
- Model (c) (Fig. 4c) is a three-dimensional explicit representation of the fracture network. A discrete model of the field test around the injection zone is analyzed taking into account 3 faults (F_{11}, F_n, F_{12}) and four bedding planes (S_7, S_8, S_9, S_{10}) (Fig. 1 and 4b). The model corresponds to a cube 6 m on a side centered on point HM1. Each fracture is modelled as a channel network identical to the Model (b).
- Model (d) (Fig. 5a) corresponds to a three-dimensional model (6 m × 6 m × 6 m) of a single fracture surrounded by a deformable rock mass. This model is used in the 3DEC hydromechanical analysis.

For each model, initial and boundary fluid pressures were set according to the natural hydrostatic pressure gradient in the rock mass (Fig. 4d and 5b). Models were fully saturated with water. For hydromechanical simulations conducted with Model (d), a vertical stress corresponding to the weight of the overburden rock mass was applied on the top boundary, with displacements fixed to zero at other boundaries (Fig. 5b). Based on previous simulations [*Cappa et al.*, 2005; *Cappa et al.*, 2006b], models size and boundary conditions were defined to have no significant effect on the numerical results.

In each simulation, a pulse test was simulated by imposing a time-dependent pressure pulse corresponding to the pulse-pressure evolution in the injection borehole (Fig. 3). For hydromechanical simulations, the calculation was stepped forward in time with the hydromechanical analysis. Within each hydraulic step, mechanical equilibrium was achieved, leading to updated effective-stress-induced changes in normal and shear displacements and resulting changes in fracture aperture.

Mechanical properties of the rock matrix and the hydromechanical properties of fractures (Tables 2) were taken from previous *in situ* and laboratory experiments [*Cappa et al.*, 2005; *Cappa et al.*, 2006b]. Based on previous evaluations of fault hydraulic permeability, the initial apertures of the fracture were set to 1×10^{-4} m [*Cappa et al.*, 2006b].

5. Modelling Results and Sensitivity Analysis

5.1. Hydraulic Modelling Results

5.1.1. Parallel Plates Flow Model Analysis

Fluid flow for a parallel plate fracture model was analysed using Model (a). When the time-lag was matched, pressure magnitude was underestimated; conversely, when the pressure magnitude was matched, the time-lag was underestimated (Fig. 6). The larger the hydraulic aperture, the greater the pressure magnitude, and the shorter the time-lag. Pressure magnitude was well captured with a hydraulic aperture of 5×10^{-5} m, while the time-lag was well matched with a smaller hydraulic aperture of 2×10^{-5} m. The aperture value of 1×10^{-4} m, obtained from previous field experiments on the site, overestimated the magnitude of pressure and underestimated the time lag. With this model, there were large differences between data and simulation results.

5.1.2. 3FLO Modelling Results: Reference Case and Sensitivity Analysis

5.1.2.1. Reference Case

In this reference case, Model (b) was used to calculate fracture hydraulic parameters. The best match to field data was obtained for a fracture storativity of 9.5×10^{-6}, a hydraulic conductivity for vertical channels of 3.6×10^{-5} m/s, and a hydraulic conductivity of horizontal channels of 4.17×10^{-7} m/s (Fig. 7 and Table 2). In this best-fit solution, the hydraulic conductivity tensor was anisotropic, and each component of the tensor was oriented as follows:

- K_h is parallel to the horizontal channels in the fracture plane and corresponds to the horizontal component;
- K_v is parallel to the dip direction of the fracture.

The anisotropy is very high. The hydraulic conductivity in the dip direction is a factor of 86.3 greater than that it is in the strike direction.

Figure 8 presents vertical and horizontal pressure profiles along the fracture for the best fit solution. Results indicated that the pressure gradient caused by the injection was asymmetric, with a radius of influence higher in the vertical direction than in the horizontal direction (Fig. 8b-d). During the pressure-increase portion at the injection point (t_1 and t_2), fluid pressure mainly propagated in the vertical channels. At the pulse-pressure peak at HM1, the radius of influence was 2.6 m in the dip direction and 1 m horizontally. During the pressure decrease portion at the injection point (t_3 and t_4), the radius of influence increased and reached 3.6 m upward, the bottom boundary and 1.6 m horizontally. Although the pressure decreased at HM1, it continued to increase, going far from the injection point.

In summary, this best-fit case showed anisotropy of the hydraulic conductivity in the fracture plane. During the pulse test, the radius of influence was asymmetric, with pressure propagating further in the dip direction than in the horizontal direction. This best-fit solution

was used as a reference case in a sensitivity study presented below, to address the importance of each hydraulic parameter, as well as the importance of the channel network geometry and the fracture network geometry with respect to the hydraulic response of the pressurized fracture in HM2.

5.1.2.2. Effects of Channel Spacing

A change in channel spacing within the fracture plane causes a significant impact on the pressure magnitude, but no significant effect on the pressure-time response (Fig. 9a). An increase in channel spacing by a factor 2 or 4 increases the magnitude of the pressure peak of about 10 kPa. The closer the channel spacing, the higher the magnitude of peak pressure.

5.1.2.3. Effects of the channel-network geometry

In the best fit solution, an orthogonal channel network was arbitrarily chosen to connect HM1 and HM2. Nevertheless, multiple representations of the channel network are possible. To estimate the effect of the channel-network orientation, channels of Model (b) were rotated by 5° and 10° clockwise. In these two cases, results show that a change in channel orientation causes a significant impact, both on the pressure magnitude and on the time lag (Fig. 9b). Pressure decreases and time-lag is overestimated.

5.1.2.4. The Effects of Fracture Network Geometry

The effects of fracture network geometry on the hydraulic response of the pressurized fault (F_{12}) were highlighted by comparing the following two numerical cases:

- Fault F_{12} exclusively (Model (b))
- Full fractures (Model (c))

Results indicate that curves are quite similar (Fig. 9c), although some difference appears in the pressure magnitude. Pressure is slightly reduced in the full-fracture model due to a slight leakage in the adjacent bedding planes. This negligible effect is due to the high contrast of the hydraulic parameters between the low-permeable bedding planes and the pressurized fracture.

5.1.2.5. Effects of Hydraulic Aperture

A variation in the fracture hydraulic aperture by a factor of 2 has a significant influence on both the magnitude of pressure and of time-lag (Fig. 10a). The lower the hydraulic aperture, the higher the magnitude of fluid pressure, and the shorter the time lag. In 3FLO, hydraulic aperture determines the channel volume in which fluid flows. Thus, for a lower hydraulic aperture, channel volume is reduced, and fluid pressure penetrates farther and faster into the fracture and contributes to increase fluid pressure at HM2.

5.1.2.6. Effects of Storativity

A variation in fracture storativity by a factor of 2 has a significant impact on both the magnitude of pressure and the time lag (Fig. 10b). The lower the storativity, the higher the magnitude of fluid pressure, and the shorter the time lag. For example, decreasing fracture storativity by a factor of 2 shortens the time lag by 0.5 seconds and increases the peak pressure by 5.5 kPa (Fig. 10b).

5.1.2.7. Effects of Hydraulic Conductivity

The effect of hydraulic conductivity was analyzed by varying the hydraulic conductivity of subvertical and horizontal channels. Figure 10c shows that a change in the hydraulic conductivity of the subvertical channels significantly shifts both the magnitude of pressure and the time lag. An increase by a factor of 2 increases the fluid pressure about 10 kPa.

Similarly, a decrease by a factor of 2 decreases the fluid pressure about 10 kPa. An increase or a decrease by a factor 2 in the hydraulic conductivity of the subvertical channels causes a shift in the pressure-time curve of approximately 0.5 seconds along the time axis.

A change in the hydraulic conductivity of the horizontal channels has an important effect on the pressure magnitude, but has no impact on the time lag between HM1 and HM2 (Fig. 10d). A change by a factor of 2 in the hydraulic conductivity of the horizontal channels induces a pressure change of 4kPa (Fig. 10d).

5.2. 3DEC Hydromechanical Modelling Results

5.2.1. Hydromechanical Effects for a Parallel Plates Flow Model

In this analysis, the effects of the hydraulically induced fracture deformation on the pressure-time response are highlighted by comparing hydraulic (see Section 5.1.1) and hydromechanical modelling results with the two parallel plate models (Fig. 4a and 5a). For the same initial hydraulic properties, an important difference appears (Fig. 11). When hydromechanical coupling is considered, the pressure magnitude decreases and time lag significantly increases as a result (Fig 11a and 11b). The increase in hydraulic aperture causes an increase in storage. As a consequence, fluid pressure is lower and penetrates more slowly into the fracture for a given well pressure and time increment.

5.2.2. Effects of the Fracture Contact Areas

Most fractures in rock are partially open, with a zone of voids between contact sections with asperities on the opposing surfaces, or bridges of intact rock [*Zimmerman et al.*, 1992; *Zimmermann and Main*, 2004]. The distribution of contact areas on rock fractures in the field is poorly known, but it is probably scale-dependant, increasing with the total length of the fracture. It is generally assumed as an initial state that a fracture is supported in part by fluid

pressure in its open sections and in part by stresses on contacting asperities [*Pyrak-Nolte and Morris*, 2000]. In this study, the effects of the number of contact areas within the fracture were examined with Model (d), considering Equation (12).

Modelling results show that the number of contact areas may have a significant impact on the hydromechanical response. A contact area ranging from 0 to 30% strongly influences the magnitude of normal displacement (Fig. 12b), but has negligible impact on the pressure-time response (Fig. 12a). The higher the number of contact areas, the lower the magnitude of normal displacement.

The difference between the normal displacement observed in the field and the simulated normal displacement results from the simplicity of the three-dimensional single fracture model. As pointed out by Cappa et al. [*2006b*], the deformability of the surrounding fractured rock mass significantly affects the hydromechanical response of the pressurized fracture. During the pulse test, hydromechanically and mechanically induced fracture shear and normal deformations occured in other discontinuities within the rock mass surrounding the tested fracture. Aperture, closure, and shearing occurring within the surrounding discontinuities resulted in additional opening of the pressurized fracture. Consequently, the change in aperture that occurs, as a result of a change in fluid pressure at a point along a fracture will depend on local effects, such as the fraction of the fracture area in contact and the stiffness of asperities, as well as global effects, such as deformation of the rock containing the fracture.

6. Discussion

6.1. Implications for In Situ Determination of Fracture Hydraulic Properties

The hydraulic analyses allowed us to identify the key parameters that influence the hydraulic response. Thess analyses indicate that the most important parameter determining the

pressure-versus-time response is the channeling. In addition, the fracture hydraulic aperture, storativity, and hydraulic conductivity are important parameters that affect the pressure magnitude and the flow time.

Our study showed that a good hydraulic connection between HM1 and HM2 is necessary to capture the pressure-time response. However, the geometry of this connection is not known in the field, and the chosen channel network geometry is one solution among multiple possibilities of representation. To best constrain the channel-network geometry, pressure changes within the fracture should be monitored in the field, with more sensors around the injection point. Thus, the orientation of channels could be evaluated more accurately by analyzing pressure changes at the additional surrounding points.

Our work also shows that the hydraulic response is highly dependent on the contrast of hydraulic conductivity between channels. In the current study, hydraulic conductivity distribution is highly anisotropic along the fracture plane. This anisotropy could be explained by a complex internal geometry of voids and by the distribution of the amount and size of the contact surface area within the fracture plane. Many studies have shown that the contact area and void space are not uniformly distributed on the fracture surface. Hakami [*1995*] shows that aperture can vary over several orders of magnitude along a fracture plane and induce flow channeling effects. Such variability in the surface roughness of a fracture induces preferential fluid flow through the highest conductive-flow channels [*Bear et al.*, 1993; *Zimmerman and Bodvarsson*, 1996].

The pressure-time response is also quite sensitive to the fracture storativity. In theory, storativity depends on both the compressibility of the fracture, the rock matrix, and the fluid as well as the height of the unsaturated zone (possibly saturated during the fluid injection) [*Rutqvist*, 1995b; *Strack*, 1989]. In our analysis, the effects of the unsaturated flow were not taken into account, although they may have a significant impact on the hydraulic response.

6.2. Comparison of Hydraulic and Hydromechanical Parallel Plates Model Analyses

For a parallel plate representation of the fracture, the differences in pressure between hydraulic and hydromechanical analyses can be directly linked to the deformability of the fracture. The difference between the hydraulic and hydromechanical responses is that the hydraulic analysis assumes that storage change results only from local changes in pressure, whereas the hydromechanical analysis assumes that nonlocal pressures can cause deformations resulting in storage changes.

Comparison between hydraulic and hydromechanical analyses demonstrates that the evaluation of the pressure-versus-time curves using only a hydraulic analysis can introduce misinterpretations in determining fracture properties. In comparing Figure 11a with Figures 10a and 10b, we can see that a 50% discrepancy occurs in the estimate of the hydraulic conductivity and storativity, between flow-only and hydromechanical calculations. To avoid such misinterpretations, pressure data must be evaluated in accordance with the fracture mechanical normal displacement measurements. Cappa et al. [*2006b*] found that mechanical measurements of transient aperture change during a pulse injection test can provide a substantially improved estimate of fracture storativity, which implies that fracture permeability can be determined more accurately from the pressure transient test. In such a case, a reasonable range of intrinsic hydraulic properties for the tested fracture could be obtained.

6.3. Contribution of the Fracture Channeling on the Hydromechanical Effects

Hydraulic modelling shows that fluid flow is strongly dependent on the number of void spaces and contact areas, which determine channeling within the fracture. In the present study, hydromechanical modelling indicates that the distribution of contact areas significantly affects

the coupling between pressure and deformation within the fracture. Channeling can reduce pressure rise, which has a significant impact on the resulting mechanical displacement. This effect has already been experimentally observed at the laboratory scale and physically linked to the discontinuity morphology [*Zimmermann et al.*, 1990; *Sibaï et al.*, 1997]. A reduced pressure rise can induce variable displacement along the fracture plane, like those observed at HM1 and HM2. Such reduced pressure rise could be emphasized by the effect of channeling on the geometry of the zone of influence for the pulse test within the fracture. This effect was analysed at the laboratory scale [*Sibaï et al.*, 1997] through hydromechanical tests performed on various natural fractures with different roughnesses and under different loading protocols. The main result of these laboratory experiments is that the predominant effect caused by channelling on hydromechanical response is the reduced pressure rise linked to the percentage of contact areas within the fracture.

7. Conclusion

Fluid flow in boreholes intersecting deformable fractures is important to problems of reservoir characterization. We conducted hydraulic and hydromechanical simulations of a pulse test applied to a highly permeable, highly deformable fracture in a carbonate reservoir to study the impact of flow parameters on the hydraulic communications in the pressurized fracture. In this study, we mainly focused our analysis on fluid pressure changes resulting from the pulse, and how the fracture parameters affected the fluid-flow process. Results indicated that pulse tests that simultaneously measure fluid pressure and mechanical displacement in fractures were a useful method for *in situ* determination of flow parameters, such as fracture hydraulic aperture, storativity, and the hydraulic conductivity tensor. During the pulse test, our measurements showed that fractures dilate and contract synchronously with transient pressure changes. The comparison between hydraulic and hydromechanical

simulation results indicated that the fracture displacement significantly affects fracture permeability and storativity, and therefore the fluid-flow process. This suggests that the simultaneous measurements of pressure and mechanical displacement signals can improve accuracy in interpreting pulse tests during reservoir characterization. Our approach also showed that channeling is at least one of the dominant parameters of fluid flow within a high-permeability fracture, like the one tested in the present study, and may also induce a high heterogeneity of flow paths along a fracture plane. In addition, the number of contact areas within the fracture may produce a significant impact on hydromechanical coupling by reducing the fracture displacement. Finally, our work showed that an appropriate numerical hydromechanical analysis of pulse injection in highly permeable fractures can be made when considering simultaneously the pressure-time and displacement–time curves, including results from both the pressure-increasing and pressure-decreasing stages as well as the possible heterogeneities induced by the distribution of contact areas. With this approach, the resolution of reservoir characterization can be substantially improved.

Acknowledgements

We are grateful for the constructive comments and recommendations of the Associate Editor, Frederick Day-Lewis, and technical review by Roger Morin (US Geological Survey), and two anonymous reviewers, who helped us to substantially improve our manuscript. The work presented in this paper was financed by contributions from the INERIS through the BCRD-DRS03 research program and the French government through the project ANR HPPP-CO2 (ref: ANR-07-PCO2-002). This work was, in part, supported by the U.S. Dept. of Energy under Contract No. DE-AC02-05CH11231.

References

Alvarez, Jr., T.A, E.J. Cording, and R.A. Milhail (1985), Hydromechanical behavior of rock joints: A reinterpretation of published experiments, In: *Rock mechanics* (Proceedings of the 35th U.S. Symposium, University of Nevada, Reno), J.J.K. Daemen and R.A Schultz, (eds). A.A. Balkema, Rotterdam, 665-671.

Barton, N.R., S. Bandis, and K. Bakhtar (1985), Strength, deformation, and conductivity coupling of rock joints, *Int. J. Rock Mech. Min. Sci. & Geomech.*, 22:121-140.

Bear, J., C-F. Tsang, and G. De Marsily (1993), Flow and Contaminant Transport in Fractured Rock, *Academic Press*, Orlando, 560 p.

Biot, M.A. (1941), General theory of three-dimensional consolidation, *J. Appl. Phys.*, 12:144-164.

Bourke, P.J. (1987), Channeling of flow through fractures in rock, In: *Proceedings of GEOVAL-1987 International Symposium*, 167-178.

Bruel, D., M.C. Cacas, E. Ledoux, and G. De Marsily (1994), Modelling storage behaviour in a fractured rock mass, *J. Hydro.*, 162:267-278.

Bruel, D. (2002), Impact of Induced Thermal Stresses During Circulation Tests in an Engineered Fractured Geothermal Reservoir. Example of the Soultz-sous-Forêts European Hot fractured Rock Project, Rhine Graben, France, *Oil & Gas Sciences and Technology – Rev. IFP*, 57(5):459-470.

Cappa F., Y. Guglielmi, P. Fénart, V. Merrien-Soukatchoff, and A. Thoraval (2005), Hydromechanical interactions in a fractured carbonate reservoir inferred from hydraulic and mechanical measurements. *Int. J. Rock. Mech. Min. Sci.*, 42:287-306.

Cappa F., Y. Guglielmi, S. Gaffet, H. Lançon, and I. Lamarque (2006a), Use of in situ fiber optic sensors to characterize highly heterogeneous elastic displacement fields in fractured rocks, *Int J Rock Mech Min Sci,* 43(4):647-654.

Cappa F., Y. Guglielmi, J. Rutqvist, C-F. Tsang, and A. Thoraval (2006b), Hydromechanical modelling of pulse tests that measure fluid pressure and fracture normal displacement at the Coaraze Laboratory site, France, *Int. J. Rock. Mech. Min. Sci.*, 43(7):1062:1082.

Cundall, P.A. (1988), Formulation of a three-dimensional distinct element model—Part I. A scheme to detect and represent contacts in a system composed of many polyhedral blocks, *Int. J. Rock Mech. Min. Sci. & Geomech. Abstr.,* 25:107-116.

Detournay, E. (1980), Hydraulic conductivity of closed rock fracture : an experimental and analytical study, in: *Proceedings of the 13th Canadian Rock Mechanics Symposium*, 168-173.

Detwiler R. L., H. Rajaram, and R. J. Glass (2002), Experimental and simulated solute transport in a partially-saturated, variable-aperture fracture, *Geophys. Res. Lett*., 29 (8), 1272, doi:10.1029/2001GL013508.

Doe, T.W., J.S.C. Long, H.K. Endo, C.R. Wilson (1982), Approaches to evaluate the permeability and porosity of fractured rock masses. In: *Proceedings of the 23rd US Rock Mechanics Symposium*, Berkeley, CA, 31–37.

Dominenco, P.A, and F.W. Schwartz (1990), Physical and Chemical Hydrogeology, *John Wiley*, 823 p.

Duveau, G., M. Sibai, X. Dunat, F. Skoczylas, and J.P. Henry (1997), Modélisation du comportement hydromécanique d'un joint rocheux sous contrainte normale, *Revue Française de Géotechnique*, 81:41-51.

Gale J. (1975), A numerical, field and laboratory study of flow in rock with deformable fractures, PhD Thesis, University of California, Berkeley, 143 p.

Gentier, S., D. Hopkins, and J. Riss (2000), Role of fracture geometry in the evolution of flow paths under stress, In: *Dynamic of fluids in fractured rock*, Geophysical Monograph 122, 169-183.

Gertsch, L.S. (1990), Changes in in situ rock joint flow characteristics caused by mechanical displacement, in: *Rocks Mechanics Contributions and Challenges*, Hustrulid and Johnson (eds), 363-370.

Goodman, R.E. (1970), Deformability of joints, in: *Proc. Symp. Determination of the In-situ Modulus of deformation of rock*, 2-7 February, Denver, Colorado. AsTm Spec. Tech. Publ., 477:174-196.

Goodman, R.E. (1974), The mechanical properties of joints, in: *Proc. 3rd. Int. Congr. International Society of Rock Mechanics*, Denver, Colorado. National Academy of Sciences, Washington, DC, 1:127-140.

Guglielmi Y., F. Cappa, J. Virieux, J. Rutqvist, and C-F. Tsang (2008), A new in situ approach for hydromechanical characterization of crustal-scale fractures: The "High-Pulse Poroelasticity Protocol" (HPPP), in: *Proceedings of the 42nd U.S. Rock Mechanics Symposium / 2nd US-Canada Rock Mechanics Symposium, San Francisco*, ARMA 08-214, 1-7.

Hakami, E. (1995), Aperture distribution of rock fractures, PhD Thesis, Royal Institute of Technology, Sweden.

Itasca Consulting Group (2003a), Inc. 3DEC 3-Dimensional Distinct Element Code. Minneapolis : ICG.

Itasca Consulting Group (2003b), Inc. 3FLO manuals. Minneapolis : ICG.

Koyama, T., N. Fardin, L. Jing, and O. Stephansson (2005), Numerical simulation of shear-induced flow anisotropy and scale-dependent aperture and transmissivity evolution of rock fracture replicas, *Int. J. Rock. Mech. Min. Sci.,* 43(1): 89-106.

Louis, C.L., and Y. Maini (1970), Determination of in situ hydraulic parameters in jointed rock, in: *Proc. 2nd Int. Congr. Rock Mechanics*, Belgrade, Inst. Dev. Water Resour., vol. I, 235-245.

Makurat, A., N. Barton, and N.S. Rad (1990), Joint conductivity variation due to normal and shear deformation, in: Barton N, Stephansson O (eds) *Rock Joints*. Balkema, Rotterdam, 535-540.

Martin C.D., C.C. Davison, and E.T. Kozak (1990), Characterizing normal stiffness and hydraulic conductivity of a major shear zone in granite. In: Barton N, Stephansson O (eds) *Rock Joints*. Balkema, Rotterdam, 549-556.

Myer, L.R. (1991), Hydromechanical and seismic properties of fractures, in: Wittke W (eds) *Proc. 7th Int. Congr. Rock. Mechanics*. Aagen, Germany. Balkema, Rotterdam, 397-404.

Moreno, L., I. Neretnieks, and T. Eriksen (1985), Analysis of some laboratory tracer runs in natural fissures, *Water Resour. Res.*, 21(7):951-958.

Moreno, L., Y.W. Tsang, C-F. Tsang, F.V. Hale, and I. Neretnieks (1988), Flow and tracer transport in a single fracture: A stochastic model and ist relation to some field observations, *Water Resour. Res.* 24(12):2033-2048.

Moreno, L., C-F. Tsang, Y.W. Tsang, and I. Neretnieks (1990), Some anomalous features of flow and solute transport arising from fracture aperture variability, *Water Resour. Res.* 26(10):2377-2391.

Murdoch, L.C., and L. Germanovitch (2006), Analysis of a deformable fracture intersecting a well. *Int. J. Num. An. Meth. Geom.*, 30, 529–561.

Neretnieks, I., T. Eriksen, and P. Tahtinen (1982), Tracer movement in a single fissure in granitic rock: Some experimental results and their interpretation, *Water Resour. Res.* 18(4), 849-858.

Olsson, R., and N. Barton (2001). An improved model for hydromechanical coupling during shearing of rock joints, *Int. J. Rock. Mech. Min. Sci.* 38:317-329.

Pyrak-Nolte, L.J., L. Myer, N.G.W. Cook, and P.A. Witherspoon (1987), Hydraulic and mechanical properties of natural fractures in low permeability rock, in: Herget G., Vongpaisal S. (eds). *Proc. 6th International Congress on Rock Mechanics*. Rotterdam: Balkema, 224-231.

Pyrak-Nolte, L.J., N.G.W. Cook, and D. Nolte (1988), Fluid percolation through single fractures, *Geophys. Res. Letters*, 15(11):1247-1250.

Pyrak-Nolte, L.J., and J.P. Morris (2000), Single fractures under normal stress: The relation between fracture specific stiffness and fluid flow, *Int. J. Rock. Mech. Min. Sci.*, 37:245-262.

Rutqvist, J. (1995a), A method to determine the stress-transmissivity relationship of joints from hydraulic field testing, in: *Proceedings of the International Congress on Rock Mechanics*, A.A Balkema, Brookfield, 1:755-758.

Rutqvist, J. (1995b), Hydraulic pulse testing of single fractures in porous and deformable rocks, *Q. J. Eng. Geol.*, 29:181-192.

Rutqvist, J., J. Noorishad, C-F. Tsang, and O. Stephansson (1998), Determination of fracture storativity in hard rocks using high-pressure injection testing, *Water Resour. Res.*, 34:2551-2560.

Rutqvist, J., and O. Stephansson (2003), The role of hydromechanical coupling in fractured rock engineering, *Hydrogeology Journal*, 11:7-40.

Schweisinger, T., and L. Murdoch (2002), Measuring changes in fracture aperture during injection to estimate characteristics of fractured rock near a well, Eos. Trans. AGU 83, no. 47: Abstract H71B-0821.

Sibaï, M., M. Haji Sotoudeh, and J.P. Henry (1997), Etude expérimentale du couplage hydromécanique de joints rocheux, *Revue Française de Géotechnique*, 81:33-39.

Snow, D.T. (1965), A parallel plate model of fractured permeable media, *PhD Thesis*, University of California, Berkeley.

Strack, O.D.L. (1989), Groundwater Mechanics, *Englewood Cliffs, New Jersey: Prentice Hall.*

Svenson, E., T. Schweisinger and L.C. Murdoch (2007), Analysis of the hydromechanical behavior of a flat-lying fracture during a slug test, *J. Hydrol.*, 347(1-2): 35-47, doi:10.1016/j.jhydrol.2007.08.020

Terzaghi, K. (1923), Die Berechning der Durchlässigkeitziffer des Tonesaus dem Verlauf Spannungserscheinungen, Akad. Der Wissenchafen in *Wien, Sitzungsberichte, Mathematisch-naturwissenschafttliche Klasse*, Part Iia, 142(3/4), 125-138.

Tse R, and D.M. Cruden (1979), Estimating joint roughness coefficients, *Int J Rock Mech Min Sci Geomech Abstr*, 32:513–23.

Tsang, C-F., and I. Neretnieks (1998), Flow channeling in heterogeneous fractured rocks, *Reviews of Geophysics*, 36(2):275-298.

Tsang, C.F. (1999), Linking thermal, hydrological, and mechanical processes fractured rocks, *Annu. Rev. Earth. Planet. Sci.*, 27:359-384.

Tsang, C-F., Y.W. Tsang, J. Birkhölzer, and L. Moreno (2001), Dynamic channeling of flow and transport in saturated and unsaturated heterogeneous media, in: *Flow and Transport Through Unsaturated Fractured Rock,* Geophysical Monograph 42, Second Edition, 33-44.

Tsang, Y.W., and C-F. Tsang (1987), Channel model of flow through fractured media, *Water Resour. Res.* 23(3):467-479.

Tsang, Y.W., C-F. Tsang, I. Neretnieks, and L. Moreno (1988), Flow and tracer transport in fractured media: A variable aperture channel model and its properties, *Water Resour. Res.* 24(12):2049-2060.

Tsang, Y.W., and C-F. Tsang (1989), Flow channeling in a single fracture as two-dimensional strongly heterogeneous permeable medium, *Water Resour. Res*., 25(9):2076-2080.

Witherspoon, P.A., J.S.Y. Wang, K. Iwai, and J.E. Gale (1980), Validity of Cubic Law for Fluid Flow in a Deformable Rock Fracture, *Water Resources Research*, 16:1016-1024.

Yang, G., N.G.W. Cook, and L.R. Myer (1989), Network modeling of flow in natural fractures, in: *Rock Mechanics as a Guide for Efficient Utilization of Natural Resources*, Khair, ed. Proceedings of 30th U.S. Rock Mechanics Symposium, A.A. Balkema, 57-63.

Zheng, Q., S.E. Dickson and Y. Guo (2008), On the appropriate "equivalent aperture" for the description of solute transport in single fractures: Laboratory-scale experiments, *Water Resour. Res.*, 44, W04502, doi:10.1029/2007WR005970.

Zimmerman, R.W., D.W. Chen, J.C.S. Long, and N.G.W. Cook (1990), Hydromechanical coupling between stress, stiffness and hydraulic conductivity of rock joints and fractures, in: Barton N. & Stephansson O. (eds). *Rock Joints Proc. Inter. Symp.*, Balkema, Leon, Norway.

Zimmerman, R.W., D.W. Chen, and N.G.W. Cook (1992), The effect of contact area on the permeability of fractures, *J. Hydrol.*, 139:79–96.

Zimmerman, R.W., and G.S. Bodvarsson (1996), Hydraulic conductivity of rock fractures, *Transport in porous media*, 23;1-30.

Zimmermann, R.W., and Y. Main (2004), Hydromechanical behaviour of fractured rocks, i:n Gueguen, Y. and Bouteca, M. (eds.), *Mechanics of fluid-saturated rocks*, Elsevier Academic Press, London, 363-422.

Notation

Nomenclature

A	Area of the element of the fracture plane (m^2)
b_h	Fracture equivalent hydraulic aperture (m)
b_{hi}	Fracture initial equivalent hydraulic aperture at the initial effective stress (m)
D	Fracture hydraulic diffusivity (m^2/s)
E_R	Young's modulus of the rock matrix (Pa)
g	Gravitational acceleration (m/s^2)
H	Hydraulic head (m)
K	Fracture hydraulic conductivity (m/s)
K_f	Fluid bulk modulus (Pa)
k_{ni}	Initial fracture normal stiffness at initial effective stress (Pa/m)
k_n	Fracture normal stiffness (Pa/m)
k_s	Fracture shear stiffness (Pa/m)
P_f	Fluid pressure (Pa)
P_0	Fluid pressure at the initial state (Pa)
q	Flow rate (m^3/s)
S	Fracture storativity (-)
S_i	Fracture intrinsic storativity (m^{-1})
T	Fracture transmissivity (m^2/s)
t	Time (s)
U_n	Fracture normal displacement (m)
U_s	Fracture shear displacement (m)
V_f	Fluid volume (m^3)
V	Fracture volume (m^3)
w	Fracture width (m)

Greek Symbols

α	Biot's effective stress constant (-)
f	Factor reflecting the influence of the roughness on the tortuosity of the flow (-)
μ	Fluid dynamic viscosity (Pa/s)
ρ	Fluid density (kg/m^3)
σ_n	Total normal stress (Pa)
σ'_{ni}	Initial effective fracture normal stress at initial conditions (Pa)
σ'_n	Effective fracture normal stress (Pa)
σ'_s	Effective fracture shear stress (Pa)

Special Symbols

∇^2	Laplace operator
Δ	Gradient

Figure captions

Figure 1. (a) Three-dimensional view of the fractured rock structure; (b) Pole plots showing the faults and bedding-plane orientations (lower hemisphere, equal area).

Figure 2. Experimental device used for hydraulic pulse tests.

Figure 3. Results of a pulse test applied to HM1 with simultaneous pressure and normal displacement measurements at HM1 and HM2 points.

Figure 4. Geometry of the three-dimensional numerical models used in the hydraulic modelling: (a) 3DEC parallel plate model of a single sub-vertical fracture (Model (a)); (b) 3FLO model of a single sub-vertical fracture represented as an orthogonal channels network (Model (b)); (c) 3FLO model of the fractures network around the HM1 injection point (Model (c)); (d) hydraulic boundary conditions used in Models (a), (b) and (c), and presented in the plane of the pressurized fracture.

Figure 5. Geometry of the three-dimensional numerical model used in the hydromechanical modelling: (a) 3DEC model of the single sub-vertical fracture embedded in the surrounding rock matrix (Model (d)); (b) hydromechanical boundary conditions presented in the plane of the fracture.

Figure 6. Results of 3DEC hydraulic analysis for a parallel plate fracture model. Figure shows the predicted and observed fluid pressure at HM2 point.

Figure 7. The 3FLO best fit solution for hydraulic modelling to in situ measurements. Figure shows the predicted and observed fluid pressure at HM2 point.

Figure 8. Pressure profiles through the fracture; (a) Sampling time steps (Δt = 1.5 s) of pressure profiles during the time-dependent pressure evolution; (b) profiles going through HM1 and HM2; (c) horizontal profiles at HM1 elevation; (d) horizontal profiles at HM2 elevation. This figure presents vertical and horizontal pressure profiles along the fracture for the best fit solution. Profiles corresponds to different stages of the pressure-time response (t_1 = 2.25 s, t_2 = 3.75 s, t_3 = 5.25 s, t_4 = 6.75 s). Pressure profiles were made with a larger fracture model (10 m × 10 m) to capture the boundaries of the radius of influence of the test.

Figure 9. 3FLO sensitivity analysis at HM2 for a pulse test applied to HM1 while varying (a) channels spacing; (b) channel orientation; (c) geometry of the fractures network.

Figure 10. 3FLO sensitivity analysis at HM2 for a pulse test applied to HM1 while varying (a) hydraulic aperture; (b) storativity; (c) hydraulic conductivity of sub-vertical channels; (d) hydraulic conductivity of horizontal channels

Figure 11. Results of coupled hydromechanical modelling: (a) comparison of the presure-versus-time curves simulated in hydraulic and hydromechanical analyses; (b) hydraulically-induced mechanical normal displacement during pulse injection

Figure 12. Effects of the amount of contact areas within the fracture on the hydromechanical response (a) pressure curves (all curves are superimposed); (b) normal displacement curves

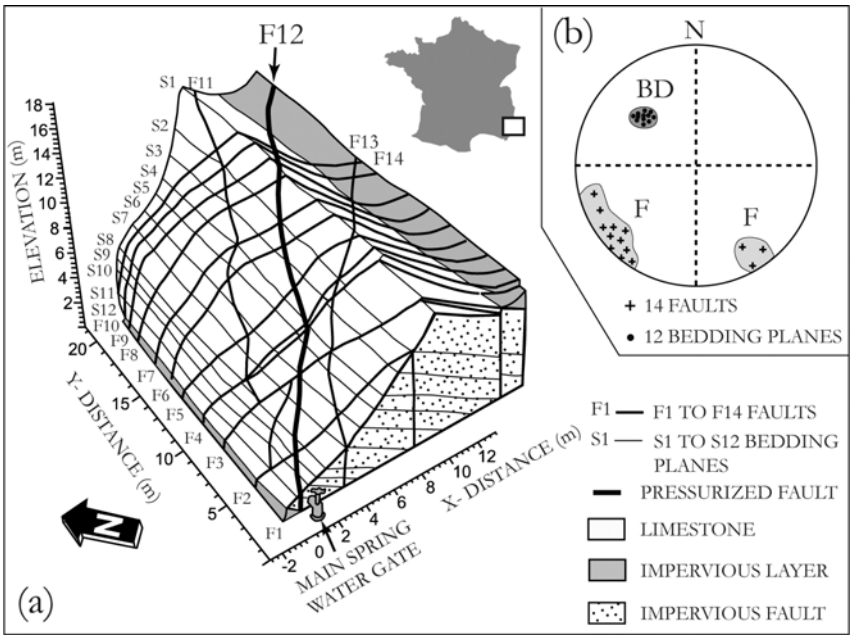
F12
S1
F11
S2
S3
S4
S5
S6
S7
S8
S9
S10
S11
S12
F10
F9
F8
F7
F6
F5
F4
F3
F2
F1
F13
F14
ELEVATION (m)
18
16
14
12
10
8
6
4
2
Y- DISTANCE (m)
20
15
10
5
X- DISTANCE (m)
-2
0
2
4
6
8
10
12
MAIN SPRING
WATER GATE
N
(a)
(b)
BD
F
F
+ 14 FAULTS
• 12 BEDDING PLANES
F1 — F1 TO F14 FAULTS
S1 — S1 TO S12 BEDDING PLANES
PRESSURIZED FAULT
LIMESTONE
IMPERVIOUS LAYER
IMPERVIOUS FAULT

Figure 1

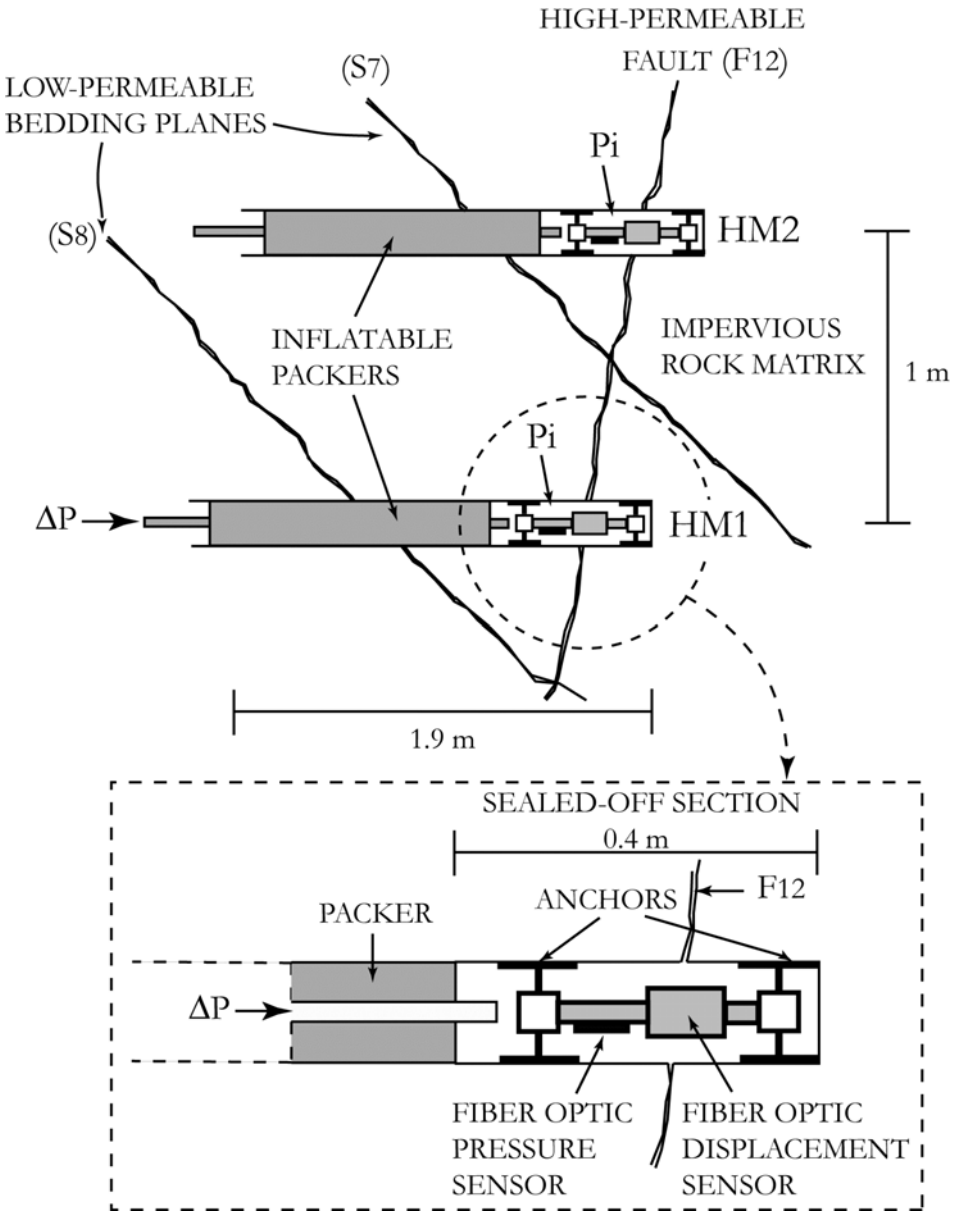
HIGH-PERMEABLE
FAULT (F12)
(S7)
LOW-PERMEABLE
BEDDING PLANES
Pi
(S8)
HM2
INFLATABLE
PACKERS
IMPERVIOUS
ROCK MATRIX
1 m
Pi
ΔP
HM1
1.9 m
SEALED-OFF SECTION
0.4 m
F12
ANCHORS
PACKER
ΔP
FIBER OPTIC
PRESSURE
SENSOR
FIBER OPTIC
DISPLACEMENT
SENSOR

Figure 2

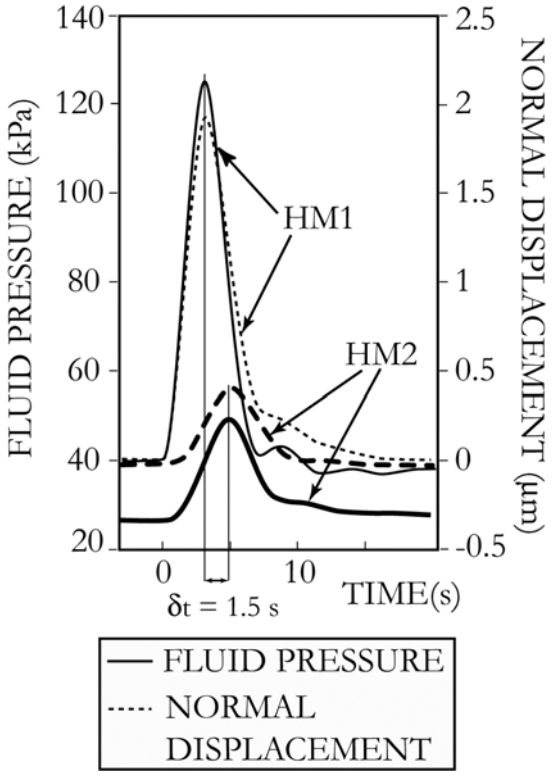
140
120
100
80
60
40
20
FLUID PRESSURE (kPa)
2.5
2
1.5
1
0.5
0
-0.5
NORMAL DISPLACEMENT (μm)
HM1
HM2
0
10
TIME(s)
δt = 1.5 s
FLUID PRESSURE
NORMAL DISPLACEMENT

Figure 3

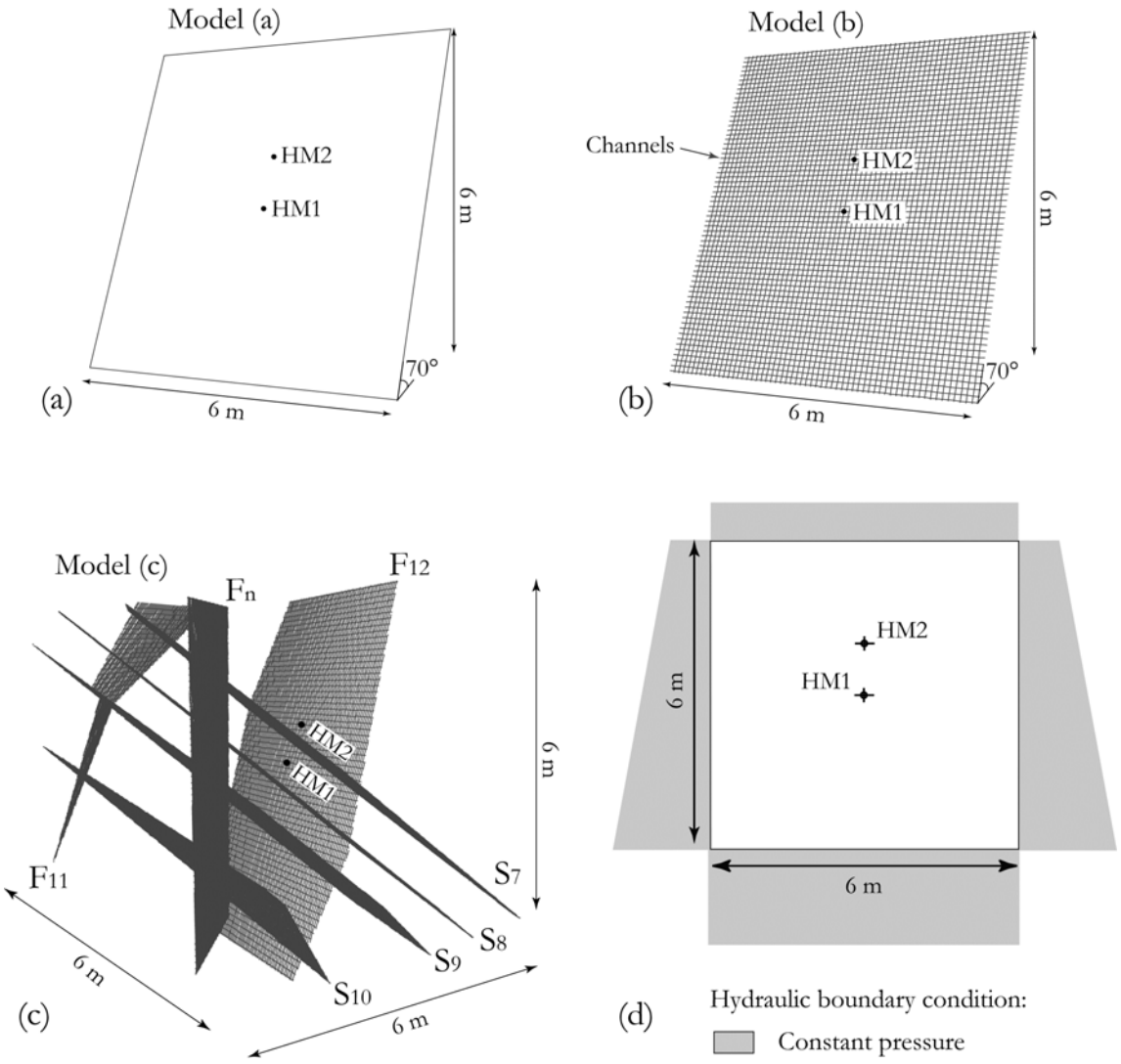
Model (a)
HM2
HM1
6 m
70°
6 m
(a)
Model (b)
Channels
HM2
HM1
6 m
70°
6 m
(b)
Model (c)
Fn
F12
HM2
HM1
6 m
F11
S7
S8
S9
S10
6 m
6 m
(c)
HM2
HM1
6 m
6 m
(d)
Hydraulic boundary condition:
Constant pressure

Figure 4

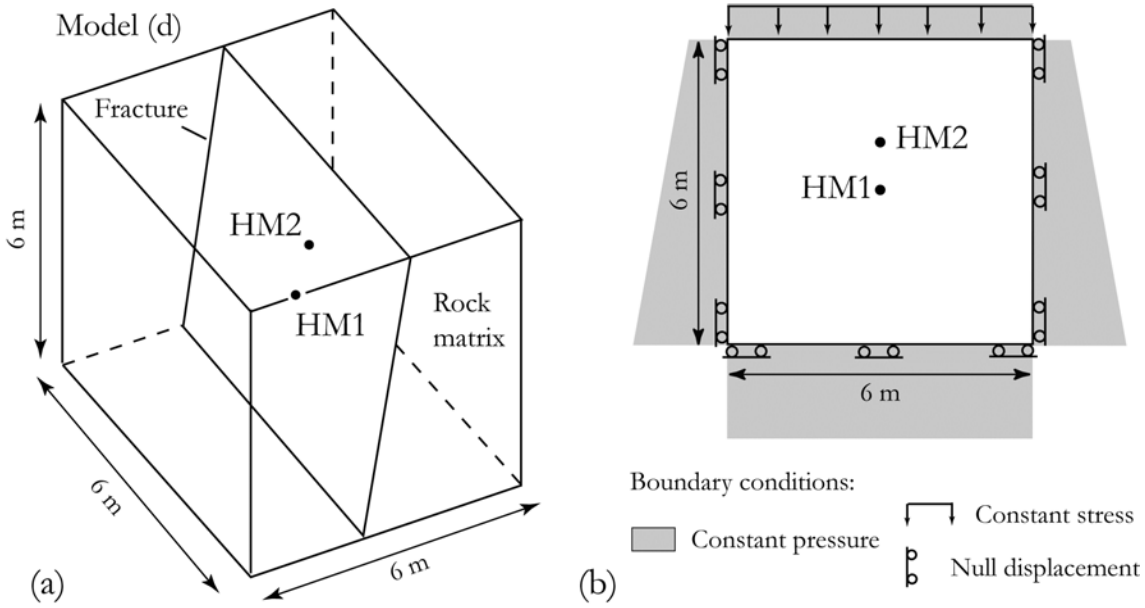
Model (d)
Fracture
HM2
HM1
Rock
matrix
6 m
6 m
6 m
(a)
HM2
HM1
6 m
6 m
(b)
Boundary conditions:
Constant pressure
Constant stress
Null displacement

Figure 5

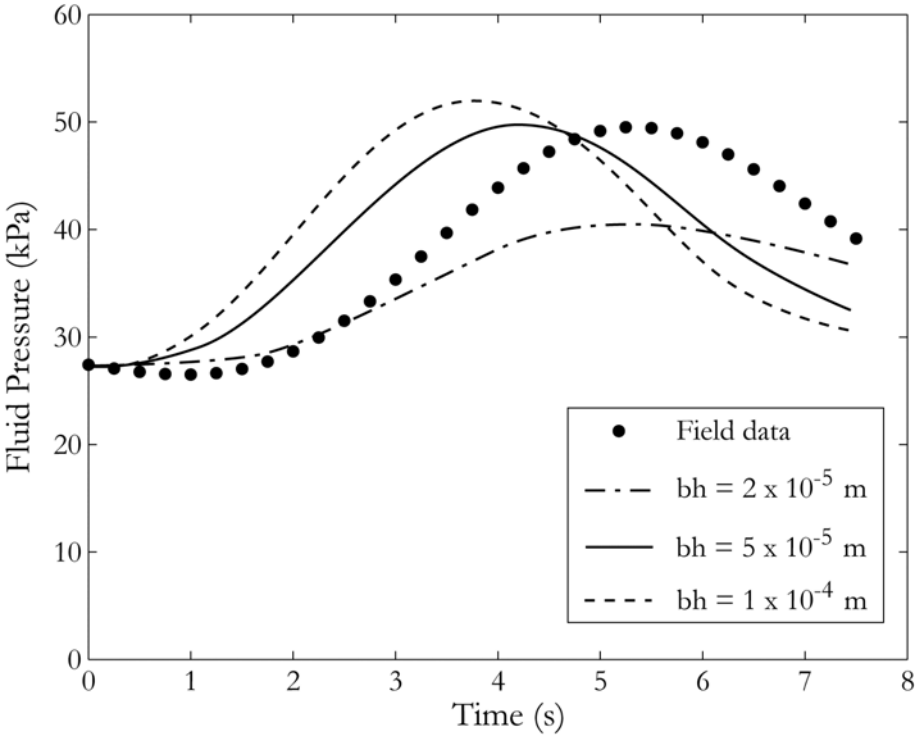
Fluid Pressure (kPa)
Time (s)
Field data
bh = 2 x 10^-5 m
bh = 5 x 10^-5 m
bh = 1 x 10^-4 m

Figure 6

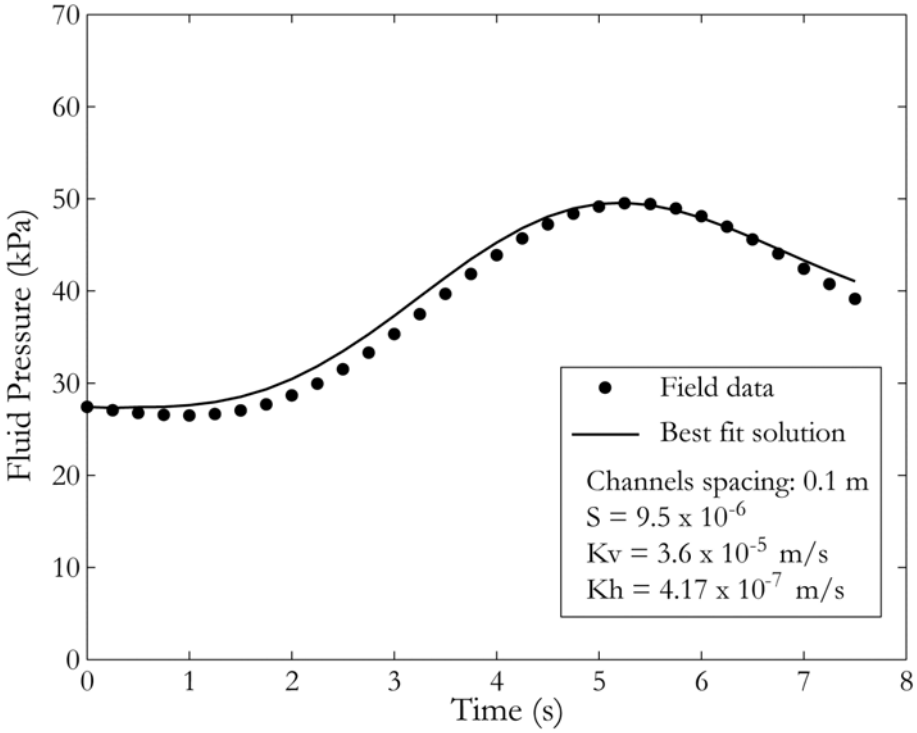
Fluid Pressure (kPa)
Time (s)
Field data
Best fit solution
Channels spacing: 0.1 m
S = 9.5 x 10-6
Kv = 3.6 x 10-5 m/s
Kh = 4.17 x 10-7 m/s

Figure 7

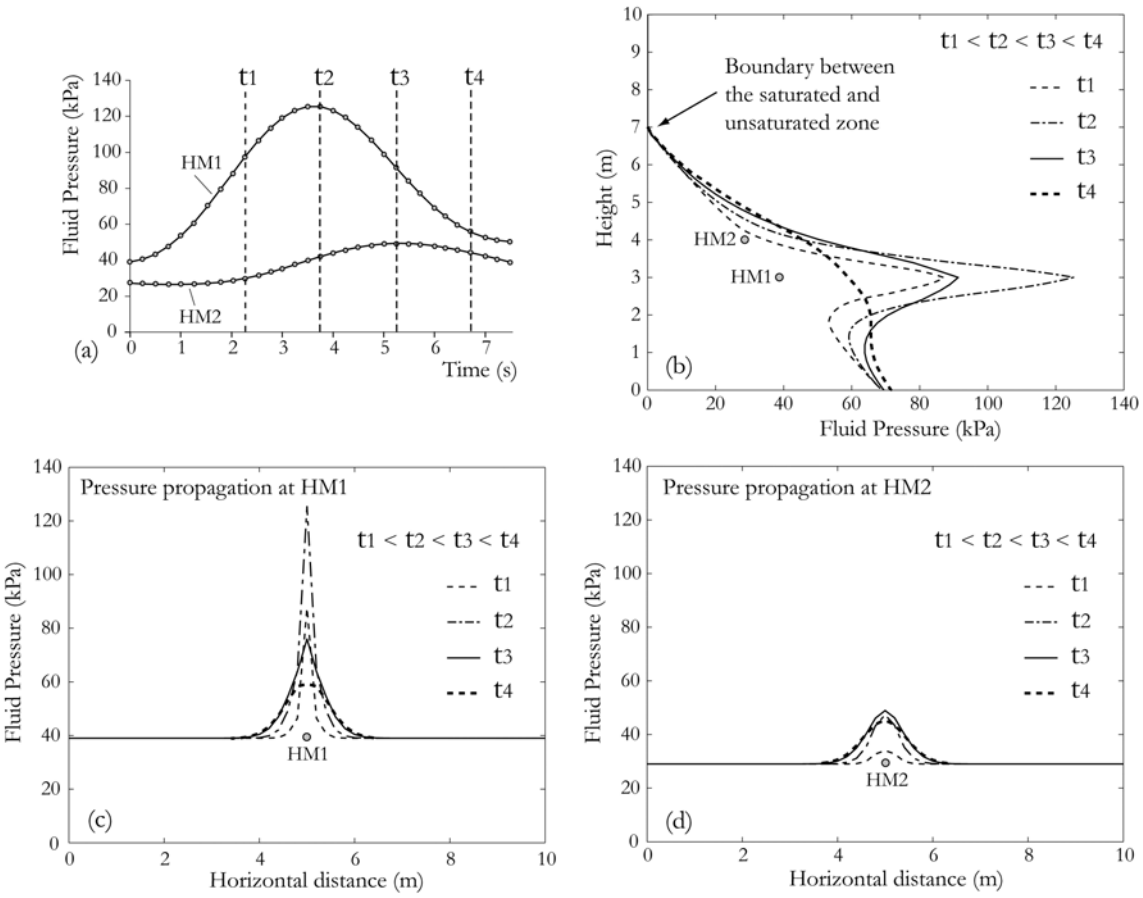
Fluid Pressure (kPa)
t1
t2
t3
t4
HM1
HM2
(a)
Time (s)
Height (m)
t1 < t2 < t3 < t4
Boundary between
the saturated and
unsaturated zone
HM2
HM1
(b)
Fluid Pressure (kPa)
Pressure propagation at HM1
t1 < t2 < t3 < t4
HM1
(c)
Horizontal distance (m)
Pressure propagation at HM2
t1 < t2 < t3 < t4
HM2
(d)
Horizontal distance (m)

Figure 8

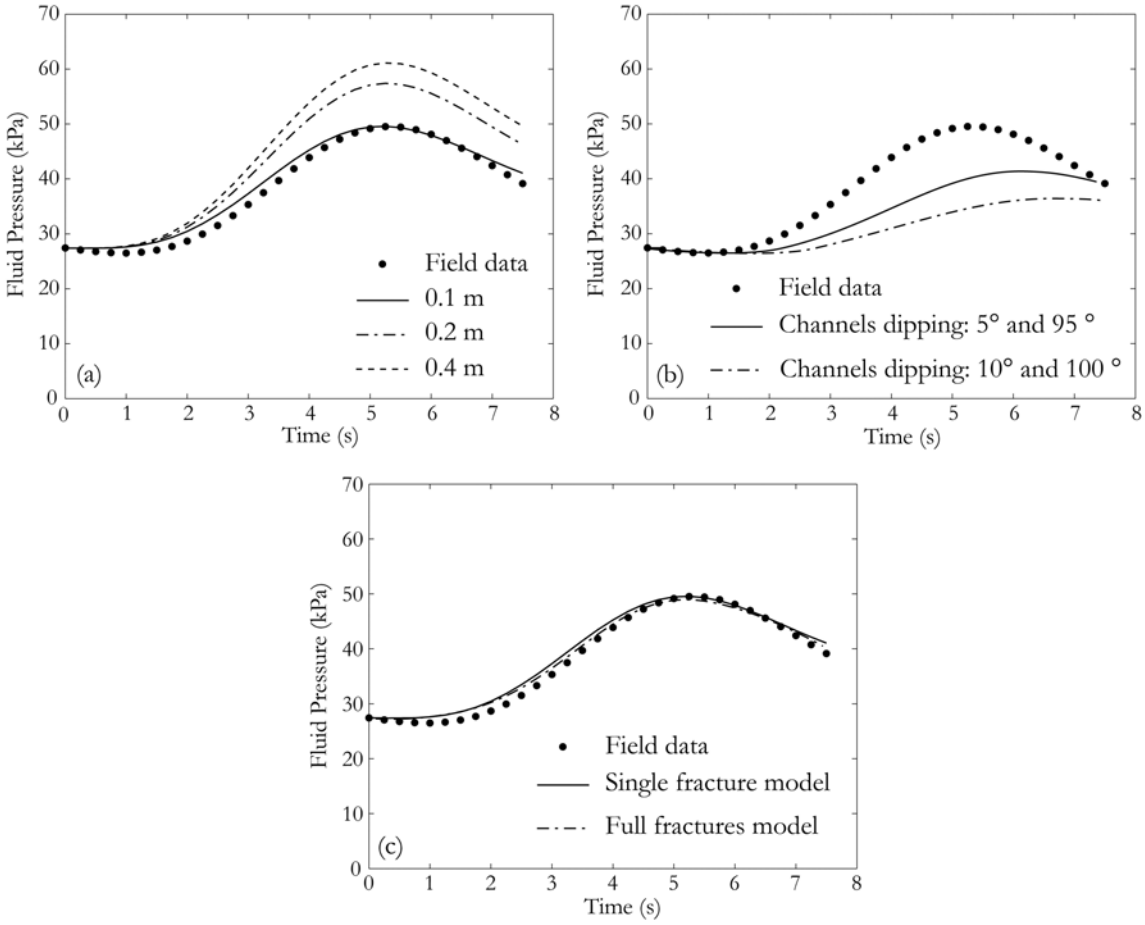
Fluid Pressure (kPa)
Time (s)
(a)
Field data
0.1 m
0.2 m
0.4 m
(b)
Field data
Channels dipping: 5° and 95 °
Channels dipping: 10° and 100 °
(c)
Field data
Single fracture model
Full fractures model

Figure 9

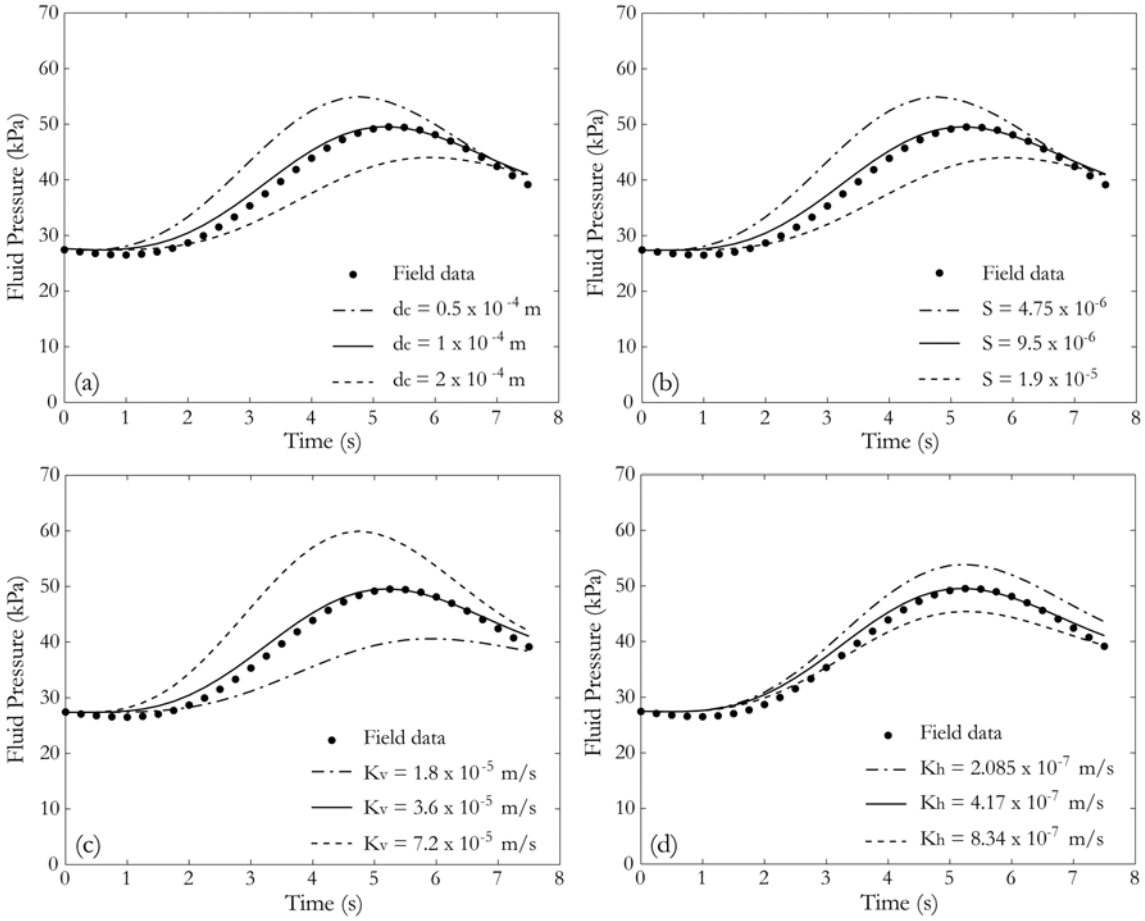
Fluid Pressure (kPa)
Time (s)
(a)
Field data
dc = 0.5 x 10^-4 m
dc = 1 x 10^-4 m
dc = 2 x 10^-4 m
(b)
Field data
S = 4.75 x 10^-6
S = 9.5 x 10^-6
S = 1.9 x 10^-5
(c)
Field data
Kv = 1.8 x 10^-5 m/s
Kv = 3.6 x 10^-5 m/s
Kv = 7.2 x 10^-5 m/s
(d)
Field data
Kh = 2.085 x 10^-7 m/s
Kh = 4.17 x 10^-7 m/s
Kh = 8.34 x 10^-7 m/s

Figure 10

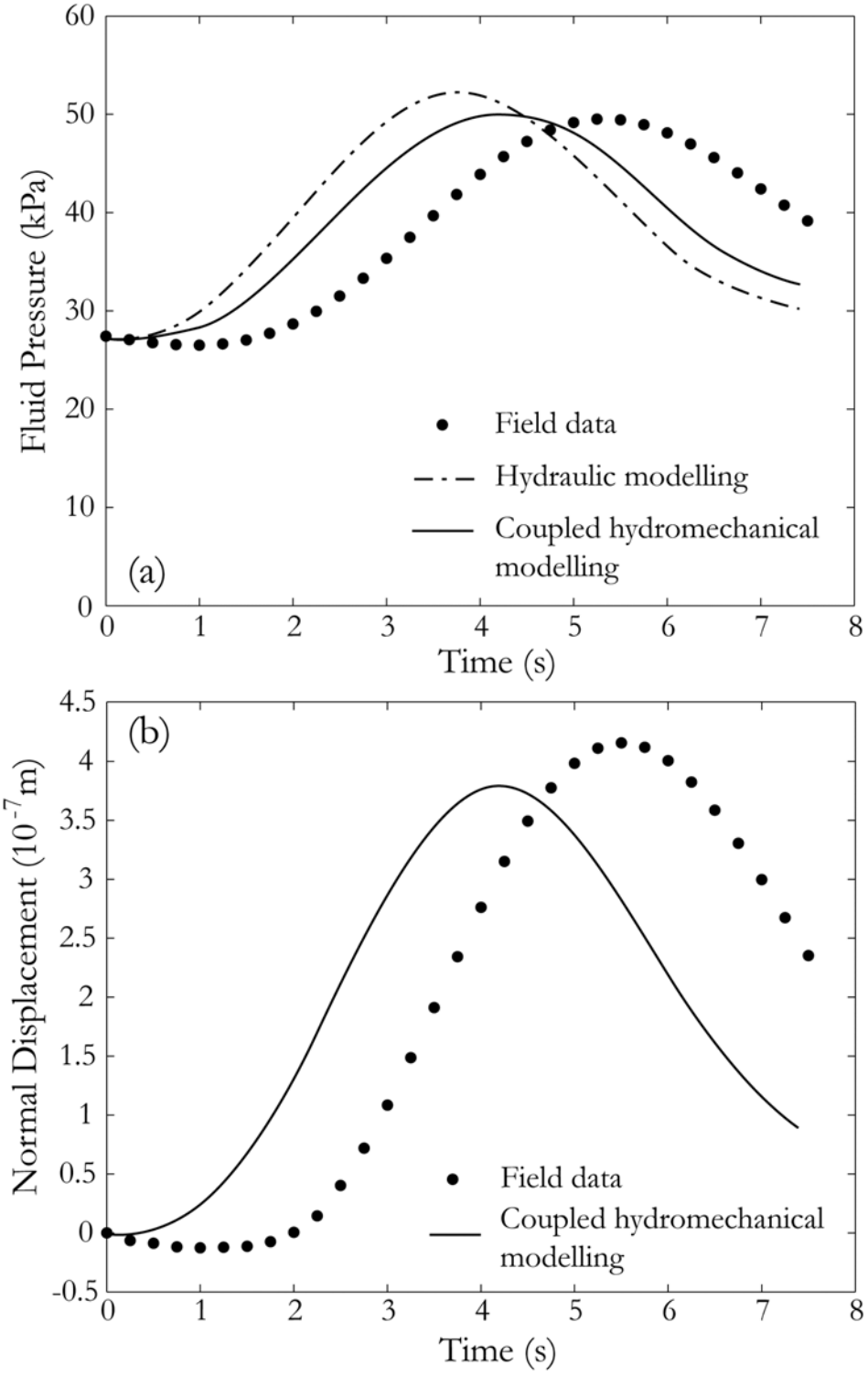
Fluid Pressure (kPa)
Time (s)
Field data
Hydraulic modelling
Coupled hydromechanical modelling
(a)
Normal Displacement (10^{-7} m)
Time (s)
Field data
Coupled hydromechanical modelling
(b)

Figure 11

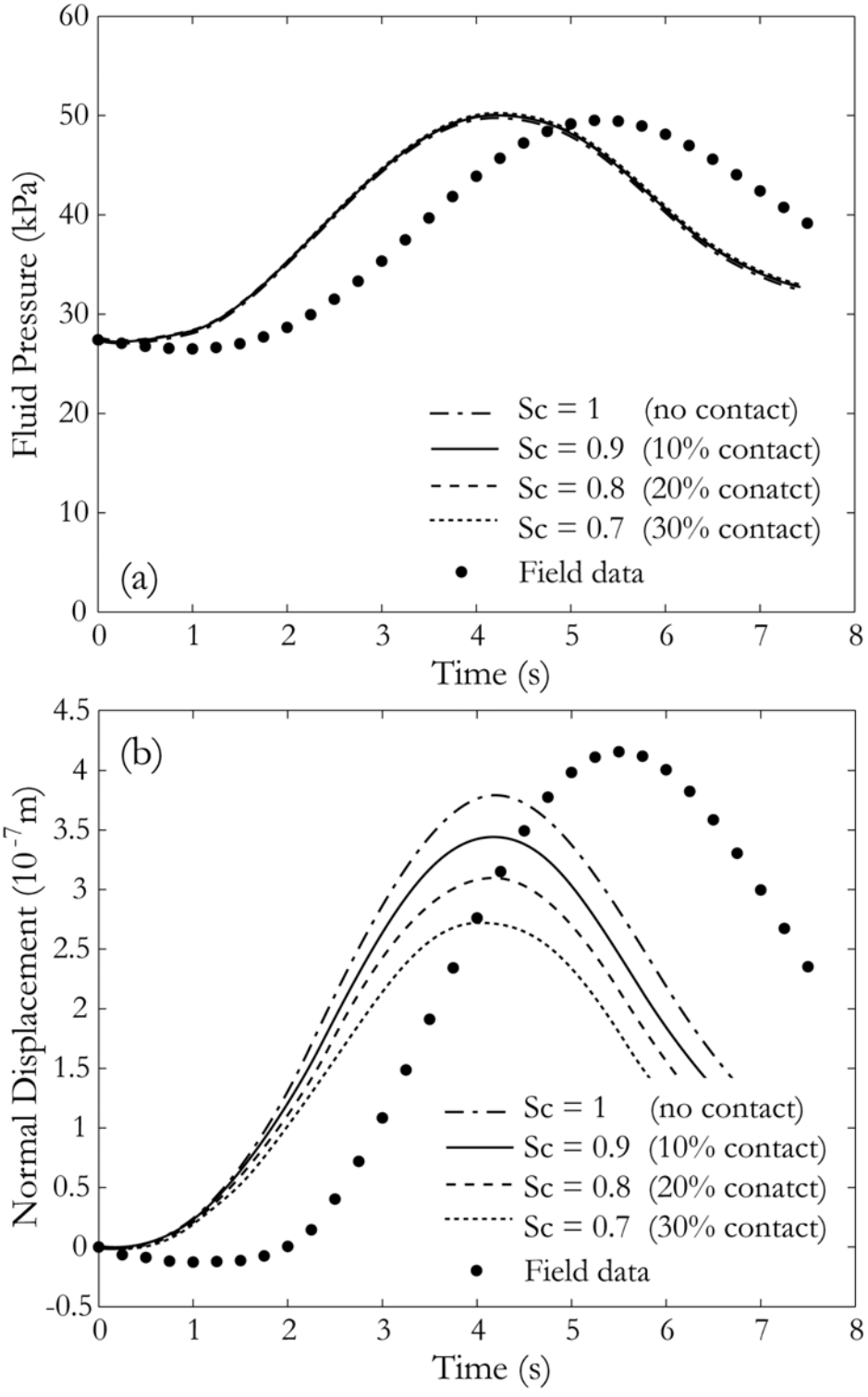
(a)
Fluid Pressure (kPa)
Time (s)
Sc = 1 (no contact)
Sc = 0.9 (10% contact)
Sc = 0.8 (20% conatct)
Sc = 0.7 (30% contact)
Field data
(b)
Normal Displacement (10^{-7} m)
Time (s)
Sc = 1 (no contact)
Sc = 0.9 (10% contact)
Sc = 0.8 (20% conatct)
Sc = 0.7 (30% contact)
Field data

Figure 12

Table 1. Codes, models, and tested parameters in each numerical approach

Numerical analysis	Hydraulic	Hydromechanical
Codes	3FLO	3DEC
Model	● a, b, c	● d
Numerical parameters tested in the sensitivity study	● Channels spacing ● Channels orientation ● Fracture hydraulic aperture ● Fracture storativity ● Fracture hydraulic conductivity ● Geometry of the fractures network	● Flow between two parallel plates ● Fracture contact areas

Table 2. Material properties used in each numerical approach

Material	Parameter	3FLO models *(b)* and *(c)*	3DEC models *(a)* and *(d)*	
			Hydraulic Simulation	Hydromechanical Simulation
Fracture	Hydraulic conductivity, K_v (m/s)	3.6×10^{-5}	8.3×10^{-3}	8.3×10^{-3}
	K_h (m/s)	4.17×10^{-7}	8.3×10^{-3}	8.3×10^{-3}
	Hydraulic aperture, b_{hi} (m)	1×10^{-4}	1×10^{-4}	1×10^{-4}
	Storativity, S_h (-)	9.5×10^{-6}	4.46×10^{-10}	4.46×10^{-10}
	Normal stiffness (GPa/m)	Not modelled	Not modelled	50[1]
	Shear stiffness (GPa/m)	Not modelled	Not modelled	5[1]
Rock matrix	Young's modulus, E_R, (GPa)	Not modelled	Not modelled	70[1]
	Poission's ratio, ν (-)	Not modelled	Not modelled	0.29[1]
	Mass density, ρ_R (kg/m^3)	Not modelled	Not modelled	2400[1]
	Permeability, k_R (m^2)	0	0	0
Fluid	Mass density, ρ_f (kg/m^3)	1000	1000	1000
	Fluid compressibility, C_f(Pa)	4.46×10^{-10}	4.46×10^{-10}	4.46×10^{-10}
	Dynamic viscosity, μ_f (Pa/s)	1×10^{-3}	1×10^{-3}	1×10^{-3}

[1] Values determined from previous evaluations of fracture hydromechanical properties (see Cappa et al., 2006b)